

# Determination of Absolute Structure of Chiral Crystals Using Three-Wave X-ray Diffraction

Ksenia Kozlovskaya <sup>1,\*</sup>, Elena Ovchinnikova <sup>1</sup>, Jun Kokubun <sup>2</sup>, Andrei Rogalev <sup>3</sup>, Fabrice Wilhelm <sup>3</sup>, Francois Guillou <sup>3</sup>, Francois de Bergevin <sup>3</sup>, Alisa F. Konstantinova <sup>4</sup> and Vladimir E. Dmitrienko <sup>4</sup>

<sup>1</sup> Faculty of Physics, M.V. Lomonosov Moscow State University, 119991 Moscow, Russia; en\_ovchinnikova@physics.msu.ru

<sup>2</sup> Faculty of Science and Technology, Tokyo University of Science, 2641 Yamazaki, Noda-shi 278-8510, Chiba-ken, Japan; kokubun@ph.noda.tus.ac.jp

<sup>3</sup> European Synchrotron Radiation Facility, 38043 Grenoble, France; rogalev@esrf.fr (A.R.); wilhelm@esrf.fr (F.W.); francoisguillou@imnu.edu.cn (F.G.); francois.bergevin@wanadoo.fr (F.d.B.)

<sup>4</sup> Federal Scientific Research Center "Crystallography and Photonics", A.V. Shubnikov Institute of Crystallography, 119333 Moscow, Russia; afkonst@mail.ru (A.F.K.); dmitrien@crys.ras.ru (V.E.D.)

\* Correspondence: kozlovskaya@physics.msu.ru; Tel.: +7-916-805-60-90

**Abstract:** We propose a new method to determine the absolute structure of chiral crystals, which is based on the chiral asymmetry of multiple scattering diffraction. It manifests as a difference in the azimuthal dependence of the forbidden Bragg reflection intensity measured with left and right circularly polarized X-ray beams. Contrary to the existing ones, the suggested method does not use X-ray anomalous dispersion. The difference between the Renninger scans with circularly polarized X-rays has been experimentally demonstrated for the 001 reflection intensities in the right- and left-handed quartz single crystals. A multi-based code on model-independent three-wave-diffraction approach has been developed for quantitative description of our experimental results. The proposed method can be applied to various structures including opaque, organic and monoatomic crystals, even with only light elements. To determine the type of isomer, the Renninger plot of a single forbidden reflection is sufficient.

**Keywords:** chirality; many-wave X-ray diffraction; renninger scan



**Citation:** Kozlovskaya, K.; Ovchinnikova, E.; Kokubun, J.; Rogalev, A.; Wilhelm, F.; Guillou, F.; de Bergevin, F.; Konstantinova, A.F.; Dmitrienko, V.E. Determination of Absolute Structure of Chiral Crystals Using Three-Wave X-ray Diffraction. *Crystals* **2021**, *11*, 1389. <https://doi.org/10.3390/cryst11111389>

Academic Editors: Mikhail Platunov and Aidar T. Gubaidullin

Received: 22 October 2021

Accepted: 11 November 2021

Published: 15 November 2021

**Publisher's Note:** MDPI stays neutral with regard to jurisdictional claims in published maps and institutional affiliations.



**Copyright:** © 2021 by the authors. Licensee MDPI, Basel, Switzerland. This article is an open access article distributed under the terms and conditions of the Creative Commons Attribution (CC BY) license (<https://creativecommons.org/licenses/by/4.0/>).

## 1. Introduction

Many biomolecules and medicines are chiral, i.e., can exist as right- or left-handed optical isomers. Such isomers are almost indistinguishable in physical and chemical properties, but differently interact with polarized light and with other chiral compounds. However, sometimes the properties of the isomers are also different. The sign of chirality is critical for the effectiveness of drugs [1,2]. The most famous chiral example is thalidomide, one optical isomer of which has a therapeutic effect, and the other one is teratogenic [3]. The determining of absolute atomic structure of chiral crystals is a significant and non-trivial problem. Visible optical methods are used only for transparent substances. In conventional X-ray diffraction the phase of a scattered wave is lost, which is why X-ray diffraction patterns always contain an inversion center and look similarly for right and left optical isomers. Thus X-ray diffraction can determine the spatial arrangement of the atoms, but don't distinguish the model of chirality. However, there are some ways to determine the chiral configuration using X-rays [4–6], and in this work we propose the new one.

Anomalous dispersion method exploits the special properties of real and imaginary parts of a scattering amplitude close to absorption edges, i.e., the incident radiation energies caused the excitation of electrons from the core levels to the empty states above the Fermi level [7–9]. However, this method can be applied to the absorption edges of atoms heavier than chlorine. As a result of anomalous scattering and absorption, the Friedel

law  $F(hkl) = F^*(-h - k - l)$  is violated, and the phase of the scattering amplitude can be determined. The diffraction pattern divides into pairs of spots which are connected by an inversion center, but differ in intensity. Anomalous X-ray dispersion is widely used for determining the absolute atomic structure of inorganic compounds, but there are a number of difficulties in applying it for crystals consisting of identical atoms (like Te) and for biologically important crystals consisting of atoms lighter than chlorine (C, H, N, O, F).

In the recent years, synchrotron radiation is widely used to solve light atom problems and decipher the organic structures commonly. For this purpose, several structural methods are developed such as MAD (multi-wave anomalous diffraction [10–12]) and SAD (single-wave anomalous diffraction [13]). Both of them are realized at the energies not very far from absorption edges, which need a presence or implantation of heavy atoms into organic structure. This requires some complicated chemical procedures. Interesting possibilities are given by the multocrystal SAD method [14], which combines the data from multiple crystals.

New possibilities to study the absolute structure of matter appeared due to the application of circularly polarized X-rays. It was first demonstrated in a study of X-ray natural circular dichroism (XNCD) in a crystal of  $\alpha$ -LiIO<sub>3</sub> [15], and since then, circular X-ray dichroism was observed in many other structures [16–19]. Recent development of XNCD was demonstrated in the visualization of chiral domain distribution by scanning over the sample surface with a small beam with circular polarization [20,21].

Another way to determine the absolute crystal structure is a study of the energy and azimuthal dependence of forbidden reflections in REXS (Resonant Elastic X-ray Scattering) [22–25]. If the energy of the incident radiation is close to the absorption edge of atoms in crystal, then the azimuthal dependence and intensities of forbidden reflections differ for right and left-handed crystals or (in opposite) for two different circular polarizations of the incident radiation. Such effects were observed in crystals with helical screw axes such as quartz (SiO<sub>2</sub>) [26], berlinite (AlPO<sub>4</sub>) [27] and tellurium [28,29]. However, the difference between the energy spectra of forbidden reflections for the right and left circularly polarized incident radiation can be observed not only in chiral crystals, but also for all substances without inversion center [30], and not only in forbidden reflections [31]. A study of a dichroism in forbidden reflections was also used for the visualization of chiral domains in DyFe<sub>3</sub>(BO<sub>3</sub>)<sub>4</sub> [32]. Both XNCD and REXS studies are performed at photon energies close to absorption edges, which can hardly be applied to crystals consisting of low Z atoms.

In the present paper, we propose a new X-ray method to determine the absolute atomic structure of crystals using only one crystal, one reflection and giving some flexibility in a choice of the wavelength of the incident radiation. However, this method is rather sophisticated because it uses a circularly polarized X-ray radiation, which is a strong restriction for its application, and, in addition, the method includes multiple-wave diffraction events.

The intensity of each Bragg reflection is composed of the main two-wave scattering and of the many-waves contributions. Figure 1 shows an example of two-wave (Bragg) reflection and roundabout three-wave reflection, for which the wave vectors of the outgoing waves are the same. Far from atomic absorption edges, two-wave scattering is not sensitive to the chirality of a sample and is not changed when the crystal rotates around the reciprocal lattice vector. If the reflection is forbidden because of crystal symmetry, two-wave contribution vanishes whereas multiple scattering part is not zero. If we perform the Renninger scan (rotating the crystal about the axis perpendicular to scattering plane [33]) using right or left circularly polarized beams, we can see that the azimuthal dependence of the forbidden reflection intensity looks different for two opposite helicities of the incident radiation or similarly for the right- or left-handed crystal samples (Figure 2). This kind of measurement is now available at the modern synchrotrons and can be realized for the forbidden Bragg reflections. To test our method, we choose two quartz crystals with right- and left-handed configuration (Figure 3). The absolute atomic structure of these crystals were optically tested, which allows for checking the correctness of our results and confirms the effectiveness of the method.

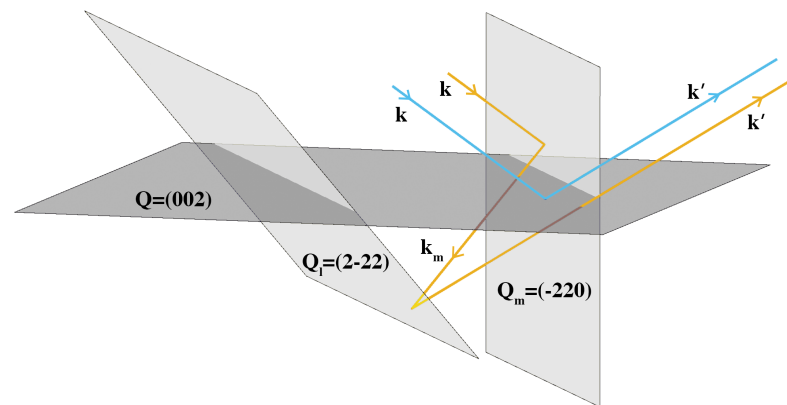


**Figure 1.** In general, the X-ray reflection intensity is composed of two-wave and three-wave parts. Here, in the case of two-wave reflection (blue line), the incident wave with the wave vector  $\mathbf{k}$  is reflected from the family of planes (002) and on the output has a wave vector  $\mathbf{k}'$ , where  $\mathbf{k}' = \mathbf{k} + \mathbf{Q}$ . In the case of three-wave reflection (orange line), the wave  $\mathbf{k}$  is reflected first by the planes  $(-220)$ , then by the planes  $(2-22)$  and on the output has the same wave vector  $\mathbf{k}'$ , where  $\mathbf{k}' = \mathbf{k}_m + \mathbf{Q} - \mathbf{Q}_m$ .

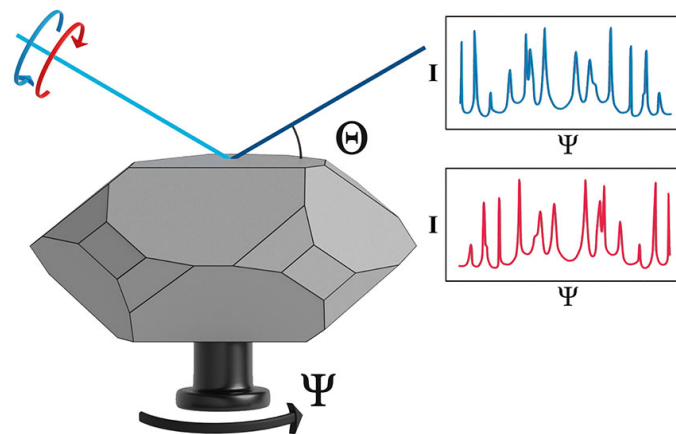


**Figure 2.** Schematic diagram of experiment. A circularly polarized X-ray radiation with an incident wave vector corresponding to the forbidden reflection falls on the crystal. The crystal rotates around the azimuthal axis by an angle of  $\Psi$ . The intensity curves look mirror-like for the left (blue curve) and right (red curve) polarizations of the incident beam.

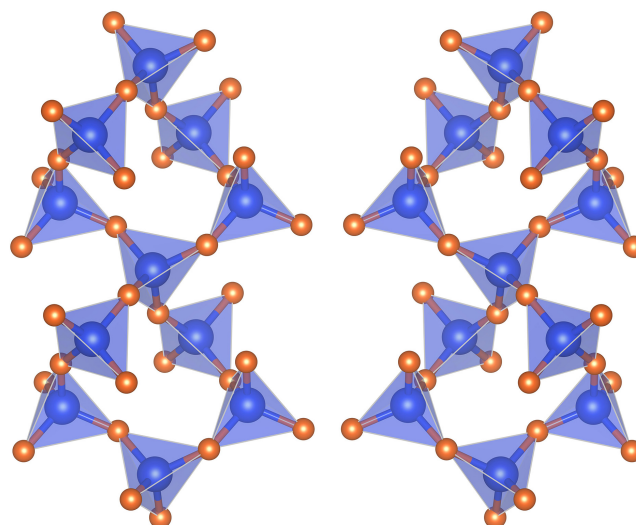


**Figure 3.** Right and left  $\alpha$ -quartz structure.

## 2. Method Description

In this section, we show that the intensity of Renninger reflections depends on the polarization of an incident radiation, providing a kind of circular dichroism, which is most obvious at the azimuthal angles between the adjacent multiple peaks. The sign of this circular dichroism is opposite for two enantiomorphous structures, which allows the determination of the absolute structure of a sample.

In conventional X-ray diffraction, the waves with eigen-polarizations  $\sigma$  and  $\pi$  do not change their polarizations during the scattering, and thus the  $\sigma$  polarization remains  $\sigma$ , and  $\pi$  transforms to  $\pi'$ . Various kinds of dichroism appear when the energy of an incident wave comes close to the absorption edges of crystal constituents. In this case, the scattering factor becomes a second rank tensor  $F_{\alpha\beta}$ , where  $\alpha$  and  $\beta$  correspond to the linear ( $\sigma$  and  $\pi$ ) or circular (*right* = + and *left* = -) polarizations. The first index corresponds to the scattered radiation, and the second corresponds to the incident radiation. However, the change of the polarization can appear even far from absorption edges due to the multiple scattering, providing a good chance to determine the absolute structure of a crystal.

Below, we shall consider the difference of the intensities of the scattered waves corresponding to the right and left circular polarizations of the incident waves:

$$\Delta(hkl) = I(hkl)_+ - I(hkl)_-. \quad (1)$$

In this paper, we do not consider the resonant processes because the energy of an incident radiation is supposed to be far from absorption edges. However, we consider the forbidden Bragg reflection, for which the scattering factor in two waves approach comes to be zero due to extinction laws of a space group. In this case, a multiple diffraction becomes most important.

Any Bragg reflection can be induced not only directly ( $\mathbf{k}' = \mathbf{k} + \mathbf{Q}$ ) but also via a multiple-wave process: first diffraction from the incident direction  $\mathbf{k}$  to an intermediate wave with the wave vector  $\mathbf{k}_m = \mathbf{k} + \mathbf{Q}_m$  and then the second diffraction process from  $\mathbf{k}_m$  to  $\mathbf{k}' = \mathbf{k}_m + \mathbf{Q} - \mathbf{Q}_m$ . We can obtain the scattering amplitude of this double-diffraction process using the infinite system of the dynamical diffraction equations [34,35]

$$(\mathbf{k}_m^2 - k^2)\mathbf{D}_m = \sum_n \chi_{m-n} (\mathbf{k}_m^2 \mathbf{D}_n - \mathbf{k}_m(\mathbf{k}_m \cdot \mathbf{D}_n)) \quad (2)$$

where  $\mathbf{D}_m$  are the Fourier harmonics of the X-ray field, and  $\chi_m$  are the Fourier harmonics of the crystal X-ray susceptibility:  $\chi_m = -r_e \frac{4\pi}{k^2 V} (F_T(\mathbf{Q}_m) + F_{res}(\mathbf{Q}_m))$ , the structure factors  $F(\mathbf{Q}_m)$  include the Thompson charge scattering and anomalous corrections but in our case the anomalous corrections are negligibly small,  $r_e$  is classical electron radius. Supposing that all  $\mathbf{D}_n$  ( $n \neq 0$ ) are small in comparison with the incident wave  $\mathbf{D}_0$  we obtain in the first approximation

$$\mathbf{D}_n = \chi_n \frac{\mathbf{k}_n^2 \mathbf{D}_0 - \mathbf{k}_n(\mathbf{k}_n \cdot \mathbf{D}_0)}{\mathbf{k}_n^2(1 - \chi_0) - k^2}. \quad (3)$$

Substituting  $\mathbf{D}_0$  and  $\mathbf{D}_n$  into Equation (2), we obtain the multiple-wave contribution to the charge scattering tensor considered reflection  $\mathbf{Q}$  [36–38]:

$$F_Q(\mathbf{e}'^* \cdot \mathbf{e}) = -r_e(\mathbf{e}'^* \cdot \mathbf{e})F(\mathbf{Q}) + \quad (4)$$

$$+ r_e^2 \frac{4\pi}{k^2 V} \sum_n F(\mathbf{Q} - \mathbf{Q}_n) F(\mathbf{Q}_n) \frac{\mathbf{k}_n^2(\mathbf{e}'^* \cdot \mathbf{e}) - (\mathbf{k}_n \cdot \mathbf{e}'^*)(\mathbf{k}_n \cdot \mathbf{e})}{\mathbf{Q}_n^2 + 2(\mathbf{k} \cdot \mathbf{Q}_n) - \mathbf{k}_n^2 \chi_0}.$$

Because of the forbidden reflection  $F(\mathbf{Q}) = 0$ , the scattering amplitude is completely determined by a sum over  $n$ .

Let us demonstrate why sharp peaks appear on the azimuthal dependence of the intensity of multiple-wave reflections. Consider the coordinate system in which  $z \parallel \mathbf{Q}$  and describe in it the direction of  $\mathbf{Q}_n$  by the angles  $\alpha_n$  and  $\phi_n$ , so that

$$\mathbf{Q}_n = |\mathbf{Q}_n|(\sin \alpha_n \cos \phi_n, \sin \alpha_n \sin \phi_n, \cos \alpha_n). \quad (5)$$

Let the incident radiation vector equal

$$\mathbf{k} = |\mathbf{k}|(\cos(\theta_B) \cos(\Psi), \cos(\theta_B) \sin(\Psi), -\sin(\theta_B)), \quad (6)$$

where  $\Psi$  describes the rotation of a scattering plane around the  $\mathbf{Q}$ . Then

$$\mathbf{k} \cdot \mathbf{Q}_n = -|\mathbf{k}| \cdot |\mathbf{Q}_n| \sin(\theta_B - \alpha_n). \quad (7)$$

During rotation around  $\mathbf{Q}$ , some atomic planes satisfy the condition  $\phi_n = \Psi$ . In this case,  $\mathbf{k} \cdot \mathbf{Q}_n = -|\mathbf{k}| \cdot |\mathbf{Q}_n| \sin(\theta_{Bn})$ ,  $|\mathbf{Q}_n| = 2|\mathbf{k}| \sin(\theta_{Bn})$ , so the denominator of the expression (4) becomes

$$\mathbf{Q}_n^2 + 2(\mathbf{k} \cdot \mathbf{Q}_n) - \mathbf{k}_n^2 \chi_0 = 4|k|^2 \sin^2(\theta_{Bn}) - 4|k|^2 \sin^2(\theta_{Bn}) - \mathbf{k}_n^2 \chi_0 = -\mathbf{k}_n^2 \chi_0. \quad (8)$$

Because  $\chi_0 \sim 10^{-5} - 10^{-6}$ ,  $\mathbf{k}_n^2 \chi_0$  has a small value, thus  $F_Q$  in (4) strongly increases, providing a multiple diffraction peak. Thus, during the rotation around  $\mathbf{Q}$  we usually see a set of multiple scattering peaks arising due to three waves diffraction from various atomic planes. However, the scattering intensity is also observed between the peaks due to the tails of various multiple scattering peaks. Certainly, the nearest peaks give the main contribution to the intensity between the peaks, but the contributions of all others also have to be considered.

Below, for simplicity, we shall neglect the absorption effects so that we calculate the difference between the forbidden reflection's intensity provided by multiple scattering of circularly polarized right and left beams as following:

$$\Delta(hkl) \sim |F(Q)_{++}|^2 + |F(Q)_{--}|^2 - |F(Q)_{+-}|^2 - |F(Q)_{-+}|^2. \quad (9)$$

Let us consider the term in (4) depending on polarizations and introduce the circular polarization vectors as follows:  $\mathbf{e}_+ = \frac{1}{\sqrt{2}}(i\mathbf{e}_\sigma + \mathbf{e}_\pi)$ ,  $\mathbf{e}_- = \frac{1}{\sqrt{2}}(i\mathbf{e}_\sigma - \mathbf{e}_\pi)$ ,  $\mathbf{e}'_+ = \frac{1}{\sqrt{2}}(i\mathbf{e}_\sigma + \mathbf{e}'_\pi)$ ,  $\mathbf{e}'_- = \frac{1}{\sqrt{2}}(i\mathbf{e}_\sigma - \mathbf{e}'_\pi)$ . Direct calculations of the polarization factors  $P_{\alpha\beta} = \mathbf{k}_n^2(\mathbf{e}'^* \cdot \mathbf{e}) - (\mathbf{k}_n \cdot \mathbf{e}'^*)(\mathbf{k}_n \cdot \mathbf{e})$  corresponding to a separate  $n$ -th multiple scattering process provides the following:

$$P_{++}^n = P_{--}^{n*} = \frac{1}{2}[k_n^2(1 + \cos 2\theta_B) - (\mathbf{k}_n \cdot \mathbf{e}_\sigma)^2 - (\mathbf{k}_n \cdot \mathbf{e}'_\pi)(\mathbf{k}_n \cdot \mathbf{e}_\pi) - i(\mathbf{k}_n \cdot \mathbf{e}'_\pi)(\mathbf{k}_n \cdot \mathbf{e}_\sigma) + i(\mathbf{k}_n \cdot \mathbf{e}_\sigma)(\mathbf{k}_n \cdot \mathbf{e}_\pi)], \quad (10)$$

$$P_{+-}^n = P_{-+}^{n*} = \frac{1}{2}[k_n^2(1 - \cos 2\theta_B) - (\mathbf{k}_n \cdot \mathbf{e}_\sigma)^2 + (\mathbf{k}_n \cdot \mathbf{e}'_\pi)(\mathbf{k}_n \cdot \mathbf{e}_\pi) - i(\mathbf{k}_n \cdot \mathbf{e}'_\pi)(\mathbf{k}_n \cdot \mathbf{e}_\sigma) - i(\mathbf{k}_n \cdot \mathbf{e}_\sigma)(\mathbf{k}_n \cdot \mathbf{e}_\pi)]. \quad (11)$$

This provides  $|F(\mathbf{Q}_n)_{++}|^2 = |F(\mathbf{Q}_n)_{--}|^2$ ,  $|F(\mathbf{Q}_n)_{+-}|^2 = |F(\mathbf{Q}_n)_{-+}|^2$ , so that  $\Delta = 0$ . This means that there is no essential circular dichroism at the azimuthal angles corresponding to the maximum of a certain multiple peak. But it is not so if we consider interference between the different multiple contributions with  $n \neq m$ , which is more important at the azimuthal angles between the main multiple peaks, where the intensity is rather small.

The intensity of the reflection is proportional to the square modulus of (4) and contains the cross terms ( $n \neq m$ ):

$$I_{\alpha\beta}^{n,m} \sim \sum_{n \neq m} \{F(\mathbf{Q} - \mathbf{Q}_n)F(\mathbf{Q}_n)P_{\alpha\beta}^n F^*(\mathbf{Q} - \mathbf{Q}_m)F(\mathbf{Q}_m)P_{\alpha\beta}^{*m} + F^*(\mathbf{Q} - \mathbf{Q}_n)F^*(\mathbf{Q}_n)P_{\alpha\beta}^{*n} F(\mathbf{Q} - \mathbf{Q}_m)F(\mathbf{Q}_m)P_{\alpha\beta}^m\} \{(\mathbf{Q}_n^2 + 2(\mathbf{k} \cdot \mathbf{Q}_n) - \mathbf{k}_n^2 \chi_0)(\mathbf{Q}_m^2 + 2(\mathbf{k} \cdot \mathbf{Q}_m) - \mathbf{k}_m^2 \chi_0)\}^{-1}. \quad (12)$$

The explicit expressions for the  $\Delta_{nm}$  are very cumbersome, and it is easier to make the numerical calculations. To demonstrate that  $\Delta \neq 0$  we can consider the interference between two nearest multiple peaks. We denote that  $F(\mathbf{Q}_i) = |F(\mathbf{Q}_i)| \exp i\Phi_i$ ,  $ReP_{\alpha\beta}^i$  and  $ImP_{\alpha\beta}^i$  are the real and imaginary parts of the polarization factors. In this case,  $\Delta$  is equal to:

$$\Delta(hkl) \sim |F(\mathbf{Q} - \mathbf{Q}_n)F(\mathbf{Q}_n)| |F(\mathbf{Q} - \mathbf{Q}_m)F(\mathbf{Q}_m)| (\sin \Phi_m \cos \Phi_n - \sin \Phi_n \cos \Phi_m) (ImP_{++}^n ReP_{++}^m + ImP_{-+}^n ReP_{-+}^m - ReP_{++}^n ImP_{++}^m - ReP_{-+}^n ImP_{-+}^m) \neq 0. \quad (13)$$

In reality, the sums in (12) contain many terms, and it is clear that  $\Delta_{nm} \neq 0$  and its value depend on a sum over many tails of multiple peaks. However, the intensity of the contributions given by (12) is much less than the intensity of the main peaks, whose magnitudes are determined by a growth of the denominators in (4) at the azimuthal angles  $\psi_n$ . Thus, it is more convenient to measure a circular dichroism at the azimuthal angles between the main multiple-wave peaks. Also, we can see from (13) that for two enantiomorphous structures, for which  $\mathbf{r} \rightarrow -\mathbf{r}$ ,  $\Phi_i \rightarrow -\Phi_i$ ,  $F(\mathbf{Q}_i) \rightarrow F^*(\mathbf{Q}_i)$ , so that  $\Delta_{nm} \rightarrow -\Delta_{nm}$ . Thus, signs of a circular dichroism corresponding to enantiomorphous structures are opposite. It opens the experimental possibility to determine an absolute structure from the measurement of the sign of the circular dichroism in a limited range of azimuthal angles.

### 3. Experiment Details

The experiments were performed at the ESRF beamline ID12, which offers full control of polarization state of incident X-rays in the photon energy range from 2 to 15 keV. For the experiments at 4.5 keV (far from the absorption edges of Si and O), we used the fundamental harmonic of radiation emitted by a helical undulator of Helios-II type with a magnetic period of 52 mm. Note that in a pure helical mode, only the fundamental harmonic is emitted on the axis of the helical undulator. We have carefully aligned the primary slits to reduce the presence of the third harmonic below the detection limit. A fixed exit monochromator was equipped with a pair of Si (111) crystals diffracting in the vertical plane. At the photon energy of the experiment the Bragg angle of the monochromator was close to 26 degree. This caused a reduction of the degree of circular polarization by a factor of 0.7. The experimental set-up is essentially a high-vacuum three-circle diffractometer operating in horizontal scattering geometry with a sample and detector arm rotations driven from outside the vacuum chamber by the Huber goniometer with a very high accuracy [30].

With this set-up, we have measured the azimuthal dependencies of the 001 forbidden reflection intensity (the Renninger scan) for the right and left circularly polarized X-rays one after the other on two quartz single crystals of opposite handedness. High quality right- and left-handed crystals (space groups  $P3_121$  and  $P3_221$ ) are the plates of about one  $\text{cm}^2$  cut perpendicular to the screw axis. Crystals were optically pre-tested, so that their absolute structures were known in advance.

### 4. Modelling of Three-Wave Multiple Reflections with Circular Polarizations

We have developed the Jmulti code for the calculations of the azimuthal dependence of the three-wave reflections intensity [39]. The Jmulti code implements the perturbation

theory calculation of the azimuthal dependencies of three-wave reflections in accordance with the expression (4). It can be used both for the linear or circular polarizations. Jmulti considers the interference between different three-wave scattering channels and can specify the indexes of reflections which give the largest contribution to the corresponding multiple peaks. This program can also be used to find the value of photon energy and azimuthal angle for which the difference in intensity  $\Delta(hkl)$  for the right- and left-handed crystals is maximal, which means that it is most convenient to determine the type of isomer.

We applied Jmulti to calculate the azimuthal dependence of multiple-wave peaks with right and left circular polarization of the incident radiation and for the right-handed and left-handed quartz crystals. The figure (Figure ??) shows the measured and calculated Renninger plots for the right-handed quartz sample, with indication of which atomic planes provide the three-waves multiple peaks. We see a good agreement between the measured and calculated curves, which confirms the correctness of the used approach taken into account only the three-waves scattering. Jmulti was also applied to simulate the three-waves multiple peaks positions on the azimuthal dependence of the intensity of 002 reflection in paratellurite [38]. The calculation showed good agreement with the experiment made at the P23 beamline of the PETRA III synchrotron facility with linear polarization [40]. It allows to rely on such calculations when simulating multi-wave diffraction in structures other than quartz.

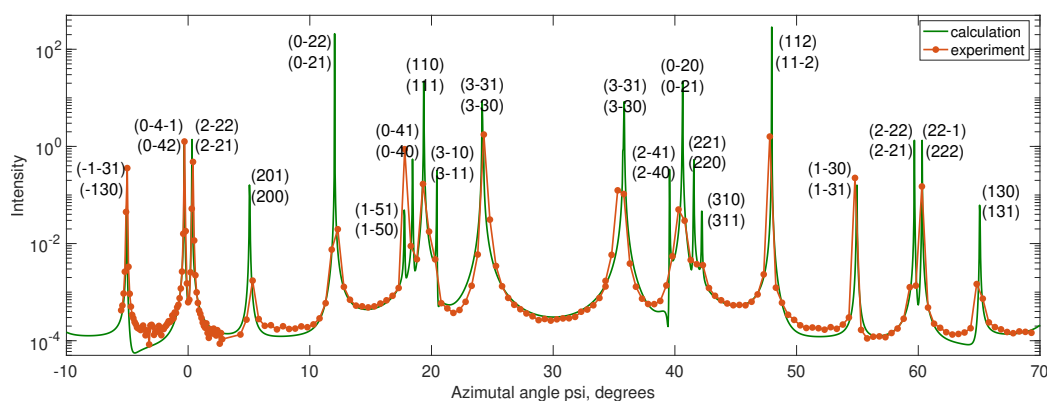


**Figure 4.** Azimuthal dependence of intensity of three-wave reflections at the photon energy  $E = 4.5$  keV in the geometry of the forbidden reflection (001) in the right  $\alpha$ -quartz.

The figure (Figure 5) shows in more details the calculated (two top pictures) and measured (bottom pictures) differences between the intensity of the 001 reflection for the right (red line) and left (blue line) circular polarization and right- and left-handed quartz crystals at the azimuthal angle between two adjacent multiple peaks in the center of the Renninger plot. The measured azimuthal dependencies of the 001 reflection intensity looks mirror-symmetric for right- and left-handed quartz, it is shown in the (Figure 5). Comparison of experimental results with calculations made it possible to determine the absolute structure of the samples and establish its agreement with the data of optical measurements. (Figure 5). We can see a mirror symmetry between the pictures corresponding to different helicities of the incident radiation or between the chirality of a sample. It means that it is possible to study only one sample to determine its absolute structure using two kinds of the incident radiation helicities.

As it was shown in [41,42], the positions of the multiple-wave peaks can be used to determine the cell parameters of the crystal with high accuracy. By varying the parameters of the crystal cell, we determined the values that would ensure the coincidence of the positions of the experimental and calculated peaks with a minimum error. The best coincidence of the peaks were obtained for the right quartz sample with the  $a = b = 4.914$  Å,  $c = 5.406$  Å, and for the left quartz with the  $a = b = 4.913$  Å,  $c = 5.404$  Å.

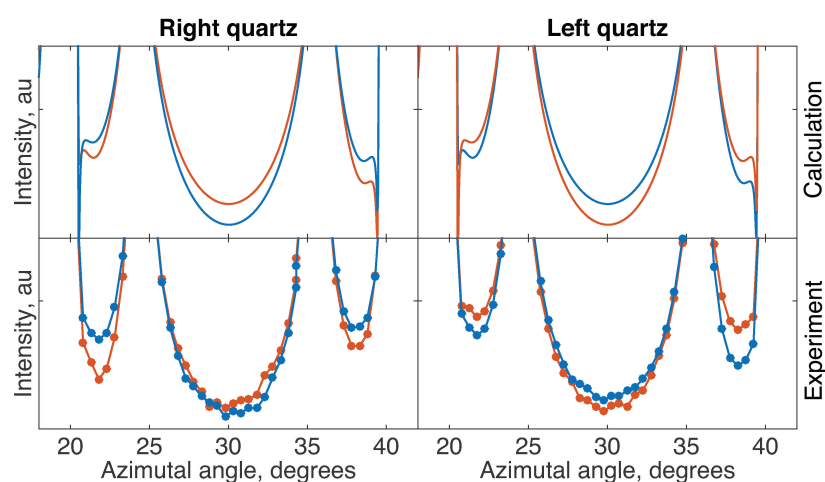


**Figure 5.** Difference in azimuthal dependence of the 001 reflection intensity of right and left quartz observed with right (red line) and left (blue line) circular polarization of x-ray beam at the azimuthal angle between the adjacent multiple-wave peaks.

## 5. Conclusions

In the paper, we described and experimentally validated a new approach for the determination of the absolute atomic structure of chiral crystals from the azimuthal dependencies of Renninger plot measured for the forbidden Bragg reflection with right and left circularly polarized X-rays. The experimental demonstration was performed on the ESRF ID12 beamline by studying the right-handed and left-handed crystals of  $\alpha$ -quartz. We show that the azimuthal curves measured with opposite circular polarizations are mirror imaged, and that there is a difference in intensities at a fixed azimuthal angle. This difference is largest between the adjacent multiple peaks. A similar effect is observed if we use only one polarization, but change the right-handed sample to the left-handed one. A theoretical approach that takes into account only three-wave multiple peaks describes all the observed features and forms the basis of the Jmulti code. It is free and allows to simulate the azimuthal dependencies of Bragg reflections for different energies of the incident radiation.

Three advantages of the proposed approach are: it is model independent, it is rather flexible in choosing the wavelength of X-rays and it needs only one forbidden reflection.

The main drawback is that it requires circularly polarized synchrotron radiation, which is not widely available. Unfortunately, the method cannot be applied in the case of structures for which there are no forbidden reflections. However we are developing further this approach to extend it to allowed reflections.

**Author Contributions:** Conceptualization, V.E.D.; software, V.E.D. and K.K.; formal analysis, E.O. and V.E.D.; investigation, A.R., F.W., F.d.B. and F.G.; sample preparation, A.F.K.; resources, A.R., V.E.D. and K.K.; data curation, K.K. and J.K.; writing—original draft preparation, K.K.; writing—review and editing, E.O., V.E.D. and A.R.; visualization, K.K.; funding acquisition, K.K. and E.O. All authors have read and agreed to the published version of the manuscript.

**Funding:** This research was partially supported by the Russian Foundation Fundamental Research project number 19-02-00483 and project number 19-52-12029.

**Institutional Review Board Statement:** Not applicable.

**Informed Consent Statement:** Not applicable.

**Data Availability Statement:** Experimental data is available upon reasonable request to the authors.

**Acknowledgments:** We acknowledge ESRF for the provision of experimental facilities via Project No. HC-1779. A.F.K. and V.E.D. were partly supported by the Ministry of Science and Higher

Education over a state contract for the Federal Research Center Crystallography and Photonics, Russian Academy of Sciences.

**Conflicts of Interest:** The authors declare no conflict of interest.

### Abbreviations

The following abbreviations are used in this manuscript:

MAD	Multi-wave anomalous diffraction
SAD	Single-wave anomalous diffraction
XNCD	X-ray natural circular dichroism
REXS	Resonant elastic X-ray scattering
ESRF	European synchrotron radiation facility

### References

1. Nguyen, L.A.; He, H.; Pham-Huy, C. Chiral Drugs: An Overview. *Int. J. Biomed. Sci.* **2006**, *2*, 85–100. [[CrossRef](#)]
2. Machida, Y.; Nishi, H. Chiral Purity in Drug Analysis. *Encycl. Anal. Chem.* **2006**. [[CrossRef](#)]
3. Stephens, T.D.; Bunde, C.J.; Fillmore, B.J. Mechanism of action in thalidomide teratogenesis. *Biochem. Pharmacol.* **2000**, *59*, 1489–1499. [[CrossRef](#)]
4. Flack, H.D.; Bernardinelli, G. Absolute structure and absolute configuration. *Acta Crystallogr. Sect. A Found. Crystallogr.* **1999**, *55*, 908–915. [[CrossRef](#)]
5. Flack, H.D. Absolute-structure determination: Past, present and future. *Chimia* **2014**, *68*, 26–30. [[CrossRef](#)]
6. Parsons, S. Determination of absolute configuration using X-ray diffraction. *Tetrahedron Asymmetry* **2017**, *28*, 1304–1313. [[CrossRef](#)]
7. Bijvoet, J.M.; Peerdeman, A.F.; Van Bommel, A.J. Determination of the absolute configuration of optically active compounds by means of X-rays. *Nature* **1951**, *168*, 271–272. [[CrossRef](#)]
8. Flack, H.; Bernardinelli, G. The Use of X-ray Crystallography to Determine Absolute Configuration. *Chirality* **2008**, *20*, 681–690. [[CrossRef](#)]
9. Materlink, G.; Sparks, C.J.; Fischer, K. *Resonant Anomalous X-ray Scattering*; Elsevier: Amsterdam, The Netherlands, 1994.
10. Smith, J.L.; Hendrickson, W.A. Multiwavelength anomalous diffraction. In *International Tables for Crystallography Vol. F*; Wiley: Hoboken, NJ, USA, 2012; Chapter 14.2, pp. 373–378. [[CrossRef](#)]
11. Stragier, H.; Cross, J.O.; Rehr, J.J.; Sorensen, L.B.; Bouldin, C.E.; Woicik, J.C. Diffraction anomalous fine structure: A new x-ray structural technique. *Phys. Rev. Lett.* **1992**, *69*, 3064–3067. [[CrossRef](#)]
12. Hodeau, J.L.; Favre-Nicolin, V.; Bos, S.; Renevier, H.; Lorenzo, E.; Berar, J.F. Resonant diffraction. *Chem. Rev.* **2001**, *101*, 1843–1867. [[CrossRef](#)]
13. Dauter, Z.; Dauter, M.; Dodson, E.J. Jolly SAD Zbigniew. *Acta Crystallogr. Sect. D* **2002**, *58*, 494–506. [[CrossRef](#)]
14. Liu, Q.; Dahmane, T.; Zhang, Z.; Assur, Z.; Brasch, J.; Shapiro, L.; Mancina, F.; Hendrickson, W.A. Structures from anomalous diffraction of native biological macromolecules. *Science* **2012**, *336*, 1033–1037. [[CrossRef](#)]
15. Goulon, J.; Goulon-Ginet, C.; Rogalev, A.; Gotte, V.; Malgrange, C.; Brouder, C.; Natoli, C.R. X-ray natural circular dichroism in a uniaxial gyrotropic single crystal of LiIO<sub>3</sub>. *J. Chem. Phys.* **1998**, *108*, 6394–6403. [[CrossRef](#)]
16. Stewart, B.; Peacock, R.D.; Alagna, L.; Prospero, T.; Turchini, S.; Glasgow, G. Circular Dichroism at the Edge: Large X-ray Natural CD in the 1s → 3d Pre-Edge Feature of 2[Co(en)<sub>3</sub>Cl<sub>3</sub>]-NaCl·6H<sub>2</sub>O. *J. Am. Chem. Soc.* **1999**, *121*, 10233–10234. [[CrossRef](#)]
17. Rogalev, A.; Goulon, J.; Wilhelm, F. X-ray detected optical activity. *Comptes Rendus Phys.* **2008**, *9*, 642–656. [[CrossRef](#)]
18. Rogalev, A.; Goulon, J.; Wilhelm, F.; Kozlovskaya, K.A.; Ovchinnikova, E.N.; Soboleva, L.V.; Konstantinova, A.F.; Dmitrienko, V.E. Investigation of X-ray natural circular dichroism in a CsCuCl<sub>3</sub> single crystal: Theory and experiment. *Crystallogr. Rep.* **2008**, *53*, 384–390. [[CrossRef](#)]
19. Oreshko, A.P.; Ovchinnikova, E.N.; Rogalev, A.; Wilhelm, F.; Mill, B.V.; Dmitrienko, V.E. X-ray natural circular dichroism in langasite crystal. *J. Synchrotron Radiat.* **2018**, *25*, 222–231. [[CrossRef](#)]
20. Platunov, M.S.; Gudim, I.A.; Ovchinnikova, E.N.; Kozlovskaya, K.A.; Wilhelm, F.; Rogalev, A.; Hen, A.; Ivanov, V.Y.; Mukhin, A.A.; Dmitrienko, V.E. X-ray natural circular dichroism imaging of multiferroic crystals. *Crystals* **2021**, *11*, 531. [[CrossRef](#)]
21. Cortijo, M.; Valentín-Pérez, Á.; Rogalev, A.; Wilhelm, F.; Saintavit, P.; Rosa, P.; Hillard, E.A. Rapid Discrimination of Crystal Handedness by X-ray Natural Circular Dichroism (XNCD) Mapping. *Chem.-Eur. J.* **2020**, *26*, 13363–13366. [[CrossRef](#)]
22. Templeton, D.H.; Templeton, L.K. Polarized X-ray absorption and double refraction in vanadyl bisacetylacetonate. *Acta Crystallogr. Sect. A* **1980**, *36*, 237–241. [[CrossRef](#)]
23. Dmitrienko, V.E. Forbidden reflections due to anisotropic X-ray susceptibility of crystals. *Acta Crystallogr. Sect. A* **1983**, *39*, 29–35. [[CrossRef](#)]
24. Dmitrienko, V.E.; Ishida, K.; Kirfel, A.; Ovchinnikova, E.N. Polarization anisotropy of x-ray atomic factors and ‘forbidden’ resonant reflections. *Acta Crystallogr. Sect. A Found. Crystallogr.* **2005**, *61*, 481–493. [[CrossRef](#)] [[PubMed](#)]
25. Mukhamedzhanov, E.K.; Borisov, M.M.; Morkovin, A.N.; Antonenko, A.A.; Oreshko, A.P.; Ovchinnikova, E.N.; Dmitrienko, V.E. Absolute intensity and phase of the resonant X-ray scattering from a germanium crystal. *JETP Lett.* **2008**, *86*, 783–787. [[CrossRef](#)]

26. Tanaka, Y.; Takeuchi, T.; Lovesey, S.W.; Knight, K.S.; Chainani, A.; Takata, Y.; Oura, M.; Senba, Y.; Ohashi, H.; Shin, S. Right handed or left handed? Forbidden X-ray diffraction reveals chirality. *Phys. Rev. Lett.* **2008**, *100*, 145502. [[CrossRef](#)]
27. Tanaka, Y.; Kojima, T.; Takata, Y.; Chainani, A.; Lovesey, S.W.; Knight, K.S.; Takeuchi, T.; Oura, M.; Senba, Y.; Ohashi, H.; et al. Determination of structural chirality of berlinite and quartz using resonant x-ray diffraction with circularly polarized x-rays. *Phys. Rev. B-Condens. Matter Mater. Phys.* **2010**, *81*, 144104. [[CrossRef](#)]
28. Tanaka, Y.; Collins, S.P.; Lovesey, S.W.; Matsunami, M.; Moriwaki, T.; Shin, S. Determination of the absolute chirality of tellurium using resonant diffraction with circularly polarized x-rays. *J. Phys. Condens. Matter* **2010**, *22*, 122201; Erratum in **2012**, *24*. [[CrossRef](#)] [[PubMed](#)]
29. Tanaka, Y.; Lovesey, S.W. Determination of absolute chirality using resonant X-ray diffraction. *Eur. Phys. J. Spec. Top.* **2012**, *208*, 67–74. [[CrossRef](#)]
30. Ovchinnikova, E.N.; Rogalev, A.; Wilhelm, F.; de Bergevin, F.; Dmitrienko, V.E.; Oreshko, A.P.; Kozlovskaya, K.A.; Bakonin, R.D. Helicity-dependent resonant X-ray scattering in  $\text{CuB}_2\text{O}_4$ . *J. Synchrotron Radiat.* **2021**, *28*, 1455–1465. [[CrossRef](#)]
31. Goulon, J.; Jaouen, N.; Rogalev, A.; Wilhelm, F.; Goulon-Ginet, C.; Brouder, C.; Joly, Y.; Ovchinnikova, E.N.; Dmitrienko, V.E. Vector part of optical activity probed with x-rays in hexagonal  $\text{ZnO}$ . *J. Phys. Condens. Matter* **2007**, *19*, 156210. [[CrossRef](#)]
32. Usui, T.; Tanaka, Y.; Nakajima, H.; Taguchi, M.; Chainani, A.; Oura, M.; Shin, S.; Katayama, N.; Sawa, H.; Wakabayashi, Y.; et al. Observation of quadrupole helix chirality and its domain structure in  $\text{DyFe}_3(\text{BO}_3)_4$ . *Nat. Mater.* **2014**, *13*, 611–618. [[CrossRef](#)]
33. Renninger, M. “Detour excitation”, a previously neglected interaction phenomenon in space lattice interferences. *Mag. Phys.* **1937**, *106*, 141–176. [[CrossRef](#)]
34. Chang, S.L. *X-Ray Multiple-Wave Diffraction*; Springer: Berlin/Heidelberg, Germany, 2004. [[CrossRef](#)]
35. Authier, A. Dynamical theory of X-ray diffraction. In *International Tables for Crystallography*; Kluwer Academic Publishers: Dordrecht, The Netherlands, 2006; Volume B, Chapter 5.1, pp. 534–551. [[CrossRef](#)]
36. Kokubun, J.; Ishida, K.; Dmitrienko, V.E. “Forbidden” Reflections Excited Owing to the Anisotropy of X-Ray Susceptibility. I. Interference with the Renninger Reflections. *J. Phys. Soc. Jpn.* **1998**, *67*, 1291–1295. [[CrossRef](#)]
37. Dmitrienko, V.E.; Ovchinnikova, E.N. Resonant X-ray Diffraction by Crystals: New Method of Studying Structure and Properties of Materials. *Crystallogr. Rep.* **2003**, *48*, S52–S68.
38. Kozlovskaya, K.A.; Kulikov, A.G.; Novikov, D.; Ovchinnikova, E.N.; Ustyugov, A.M.; Dmitrienko, V.E. Handling of Multiple-Wave Effects in the Measurement of Forbidden X-Ray Reflections in  $\text{TeO}_2$ . *Cryst. Res. Technol.* **2021**, *56*, 2000195. [[CrossRef](#)]
39. Kozlovskaya, K.A.; Ustyugov, A.; Ivanov, S.V.; Ovchinnikova, E.N.; Kulikov, A.G.; Rogalev, A. Jmulti-software for calculation of azimuth-energy maps of the intensity of three-wave x-ray reflections. *Mem. Fac. Phys. Lomonosov Mosc. State Univ.* **2020**, *6*, 2060501.
40. Ovchinnikova, E.; Novikov, D.; Zschornak, M.; Kulikov, A.; Dmitrienko, V.; Oreshko, A.; Blagov, A.; Marchenkov, N.; Borisov, M.; Khadiev, A.; et al. Forbidden reflections in  $\text{TeO}_2$  in the vicinity of the Te L1 absorption edge. *Crystals* **2020**, *10*, 719. [[CrossRef](#)]
41. Bevis, M.; Fearon, E.O.; Rowlands, P.C. The accurate determination of lattice parameters and crystal orientations from Kossel patterns. *Phys. Status Solidi A* **1970**, *1*, 653–659. [[CrossRef](#)]
42. Ullrich, H.J. Progress in the field of Kossel and pseudo-Kossel technique. *Mikrochim. Acta* **1990**, *101*, 19–24. [[CrossRef](#)]